RARE METALS

LETTER

Ultra-high-energy lithium-ion batteries enabled by aligned structured thick electrode design

Chao-Chao Zhou, Zhi Su* , **Xin-Lei Gao, Rui Cao, Shi-Chun Yang, Xin-Hua Liu***

Battery manufacturing holds great promise to build high-performance electrodes with fine-controlled microstructure, geometry and thickness. However, thick electrodes face concomitant challenge of the sluggish transport of both electrons and Li ions. Here, we present a thick electrode with an aligned structure, as an alternative to achieve high-energy lithium-ion batteries. The freeze-drying process with the aid of gum binder and single-walled carbon nanotubes (SWCNT) is originally developed for preparing the $LiNi_{0.8}Co_{0.1}Mn_{0.1}O_2$ (NCM811)-based aligned structured thick electrode as the representative cathode electrode material. The 1-mm-thick cathode with mass loading of 101 mg·cm^{-2} achieves a high specific capacity of 203.4 mAh·g^{-1}. Moreover, the as-prepared ultra-thick electrodes with a high mass loading of 538 mg·cm^{-2} and high active material content of 99.5 wt% are successfully demonstrated, delivering an extremely high areal capacity of 93.4 mAh·cm^{-2}, which represents a > 30-times improvement

compared to that of the commercial electrode. This design opens an effective avenue for greener, scalable and sustainable manufacturing processes toward energy storage devices and other related practical applications.

To develop high-performance lithium-ion batteries (LIBs), much effect has been focused on exploring novel electrode active materials aiming to replace the commercial LIBs used in 3C electronics, electric vehicles (EVs) and stationary grids, whereas the equally efficient approach to improve the electrochemical performances of LIBs via designing new battery geometries with scalable manufacture engineering attracted less attention [1–3]. In presently commercial LIBs, the fabrication process includes the stacking and calendaring of the repeatable sandwiched layers of cathode, separator and anode [4]. In the typical electrode slurry coating process, polyvinylidene fluoride binder (PVDF) is used as the binder and dispersed in the solvent of N-methyl-2-pyrrolidone (NMP). Unfortunately, both PVDF and NMP are environmentally unfriendly with high cost, and NMP removing takes more time and energy consuming than other solvents (i.e., water). Additionally, a "top-down" [5] film consolidation process is proposed, in which a dense layer or "crust" appears on the drying slurry surface and grows down, finally it reaches the electrode collector interface. Moreover, higher temperatures negatively influence electrode adhesion ability to the current collector due to binder depletion at the electrode collector interface [6]. Therefore, there is much space to improve the energy density of LIBs by increasing the thickness of structured electrodes toward binder-based manufacturing process by employing water-soluble, inexpensive and eco-friendly binders [7, 8].

The recent studies have shown that the thickness of the electrodes scales linearly with energy capacity for a given

C.-C. Zhou, Z. Su*
College of Chemistry and Chemical Engineering, Xinjiang Normal University, Urumqi 830054, China
e-mail: suzhixj@sina.com

X.-L. Gao, R. Cao, S.-C. Yang, X.-H. Liu*
School of Transportation Science and Engineering, Beihang University, Beijing 100191, China
e-mail: liuxinhua19@buaa.edu.cn

X.-H. Liu
Dyson School of Design Engineering, Imperial College London, South Kensington Campus, London SW7 2AZ, UK

areal footprint, thus, designed thick electrodes with resulting high mass loading is considered as effective approach to improve the energy density of LIBs, save the fabrication time and processing cost [9–12]. Currently, the thickness of the cathode and the anode electrodes are both limited between 50 and 100 μm [13]. Given the conventional manufacturing process, the prepared thick electrodes suffer from mechanical properties (mainly their brittle behavior and poor adhesion to the current collectors) and poor electrochemical kinetics (caused by ultra-long Li-ion transport pathway and high resistance of the Li ion diffusion in ultra-thick electrodes, especially for the cells used in EVs and operated at high rates) [14–17]. Hence, new manufacture strategies to prepare microstructured thick electrodes are needed to develop high-energy LIBs with improved electrode thickness > 100 μm and areal capacity > 3 mAh·cm^{-2} [18–22].

It is reported that the tortuosity and the resulting electrochemical performances are heavily affected by the microstructure of the electrodes [23–25]. Effects have been taken to obtain low-tortuosity electrodes, mainly focusing on designing multimodal, hierarchical and aligned porous network to achieve high performance [26–29]. As a typical example, the magnetic field-controlled assembly of LiCoO$_2$ (LCO) electro-active material into directional alignments have been developed to achieve thick electrodes with low tortuosity and high performance. However, the thick LiCoO$_2$ cathode only has a limited area capacity of 12 mAh·cm^{-2} [30, 31]. Although the construction of aligned microstructured electrode has been demonstrated as an efficient approach to accelerate the electron and ion transport in thick electrodes, the thickness of electrodes is still limited to the submillimeter range due to the slurry rheological issues, and the areal capacity can hardly be improved because of binder/carbon black network collapse and crack formation during thick electrode manufacturing [32].

In this work, a freeze-drying route to fabricate directional microchannel aligned structured ultra-thick electrode to reduce the tortuosity for high areal capacity cathode was proposed. The highly aligned ultra-thick battery electrode, which contains mixed natural gum binder, single-walled carbon nanotubes (SWCNT) and active materials of LiNi$_{0.8}$Co$_{0.1}$Mn$_{0.1}$O$_2$ (NCM811), leads to a thickness up to 3 mm with a mass loading up to 538 mg·cm^{-2}. Owing to the well-aligned microchannels in ultra-thick NCM811-based cathodes, the ion transportation can be largely enhanced compared to that of the conventional electrodes with randomly dispersed active material particles. The areal capacity of as-prepared NCM811 cathode can reach up to 93.4 mAh·cm^{-2} with high mass loading of 538 mg·cm^{-2}, which is, to the authors' best knowledge, the highest reported value presently.

The drying process of NCM-based cathode electrodes film sitting on top of Al current collector is illustrated in Fig. 1. Typically, the electrodes are commonly manufactured by coating a current collector (metal foil) with a slurry mixture of active material (NCM811, in this work) particles, conductive agent (carbon black (CB)), polymer binder (polyvinylidene fluoride (PVDF)) and solvent (N-methyl-2-pyrrolidone (NMP)), as schematically described in Fig. 1a–c. The manufacturing process, such as drying process, is a crucial step in electrode preparation as it can affect the component distribution and the microstructure within the electrode. During the drying process, the NCM811 particles are in suspension in the slurry mixture while the PVDF binder is dissolved in the NMP solvent. Then the NMP solvent starts evaporating from the top surface of the electrode coating and the film trends to shrink until the NCM811 particles are in contact with the current collector and the electrode thickness stops decreasing. The evaporation further continues and the pore space between particles starts emptying. Finally, all the solvent can be removed and the wet pore space can turn into dry pore space. The manufacturing process significantly affects the final electrode microstructure and thickness; therefore, the electrochemical and mechanical properties of the resulting electrodes remain challenge.

As shown in Fig. S1, the removal of the NMP solvent from the film surface causes crack of the electrode film, and the electrode losses contract with the current collector. Figure S2a presents scanning electron microscopy (SEM) images of the cross section of electrode (PVDF + NCM + CB Super P) prepared by conventional thermal drying applying NMP solvent. And the enrichment of binder in the upper electrode regions is shown in Fig. S2b. More NCM811 particles can be found in bottom layer of the electrode (Fig. S2c). SEM–energy-dispersive X-ray spectroscopy (SEM–EDX) mapping of the electrode can further prove this point. Herein, the phenomenas, such as binder migration, can further lead to negative effect in cell electrochemical performances (e.g., capacity fade) or mechanical failure (e.g., electrode delamination from the current collector).

To improve the binder homogeneities and the adhesion of the electrode to the current collector, effect should be taken upon optimization of polymer binder or carbon conducting agent as well as manufacturing conditions. Recently, natural gum binders have been developed to increase the slurry viscosity. Here, SWCNT was used as conducting agent, and a mixed gum binder was used to prepare the gel electrode because of the synergistic interactions between xanthan gum and guar gum (XG). However, there remain challenges to prepare thick electrode. Figure S3 shows photograph, and Fig. S4 shows SEM images of the thick electrodes (XG + NCM + SWCNT)
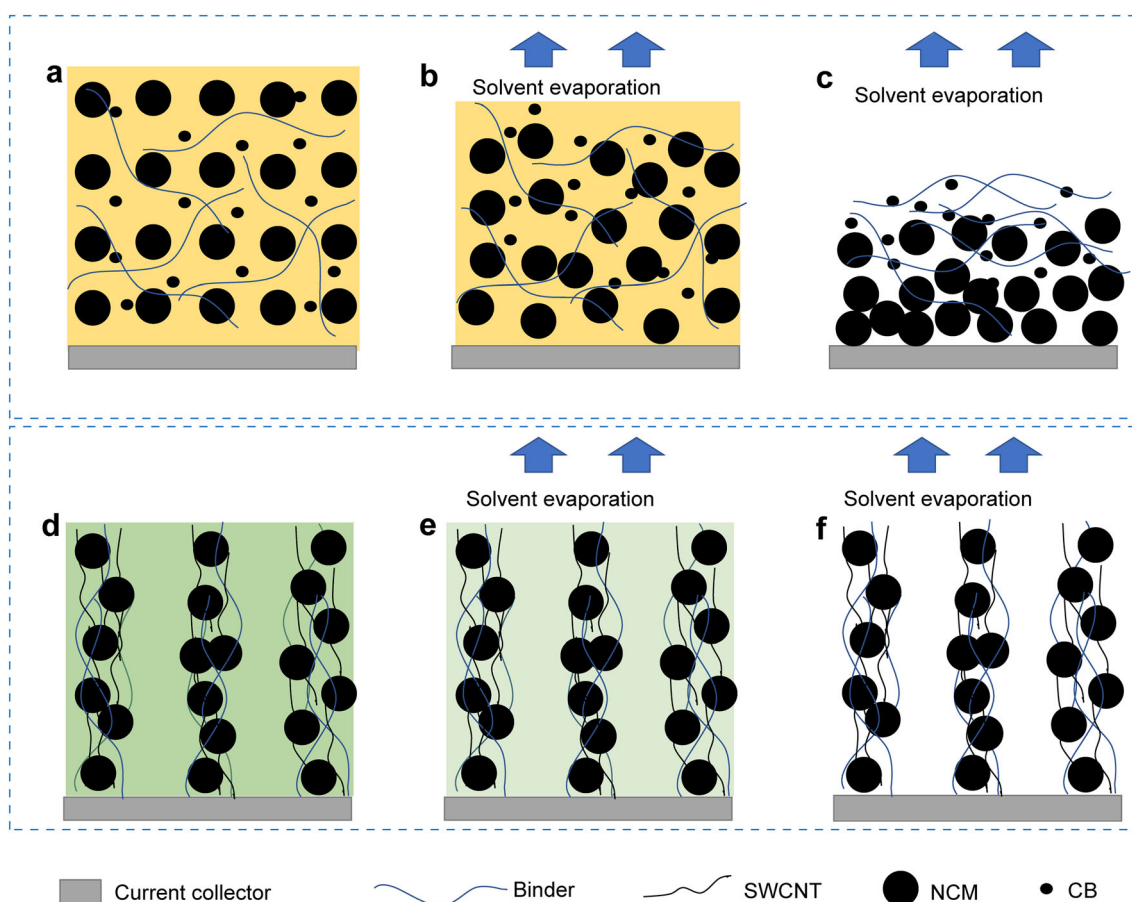
Fig. 1 Illustration of drying process of a NCM-based cathode electrode film sitting on top of Al current collector: **a–c** conventional drying process; **d–f** aligned structured electrode via freeze-drying (backgrounds representing solvent, orange: NMP solvent; green: water solvent)

with mass loading of about 300 mg·cm^{-2} prepared by conventional thermal drying.

As shown in Fig. 1d–f, it is possible to prepare ultra-thick electrode by using gum binder and applying freeze-drying process. Experimental results also confirmed that the thick electrode can be obtained by employing gum binder and freeze-drying process. Based on SEM images of the freeze-dried electrodes using a single binder in Fig. S5, the aligned and porous structure can be observed. The aligned structure can be obtained by using single xanthan gum or guar gum binder, for which the alignment can be greatly improved after combining with freeze-drying treatment. Therefore, the fine aligned microstructure can be attributed to synergetic effect of the xanthan–guar (XG) gum binder and freeze-drying. As shown in Figs. 2, S6, SEM and SEM–EDX images demonstrate that the NCM811 particles uniformly distributed throughout the whole aligned structured cathode, indicating the uniform distributions of NCM811, XG gum binder and SWCNT. Through a freeze-drying process, we can completely duplicate the vertically aligned structured ultra-thick

electrode with the thickness from about 1 up to 3 mm (more than 30 times that of the existing electrodes).

This fine aligned ultra-thick electrode can be greatly attributed to the synergistic reaction mechanism of xanthan gum and guar gum. According to the literature, xanthan gum possesses a double helix network with a hydrophobic backbone and thus exists a series of inter/intramolecular hydrogen bonding interactions [33, 34], and guar gum is a polysaccharide derived from the endosperm of seeds of Cyamopsis tetragonolobus. Results show that at a total polysaccharide concentration of 1 wt%, the highest synergism occurs at a xanthan gum/guar bean gum volume blending ratio of 1:2. The mixed hydrogels with XG binder, NCM811 and SWCNT were then freeze-dried to prepare ultra-thick electrodes. The consequence of binder homogeneities includes fine adhesion of the electrode to the current collector, decreased electrical resistivity and increased cell capacity. The highly aligned microstructured electrode with low-tortuosity pores can accelerate ion transport and further ensure excellent kinetic properties of the as-prepared ultra-thick electrode. Here, both xanthan
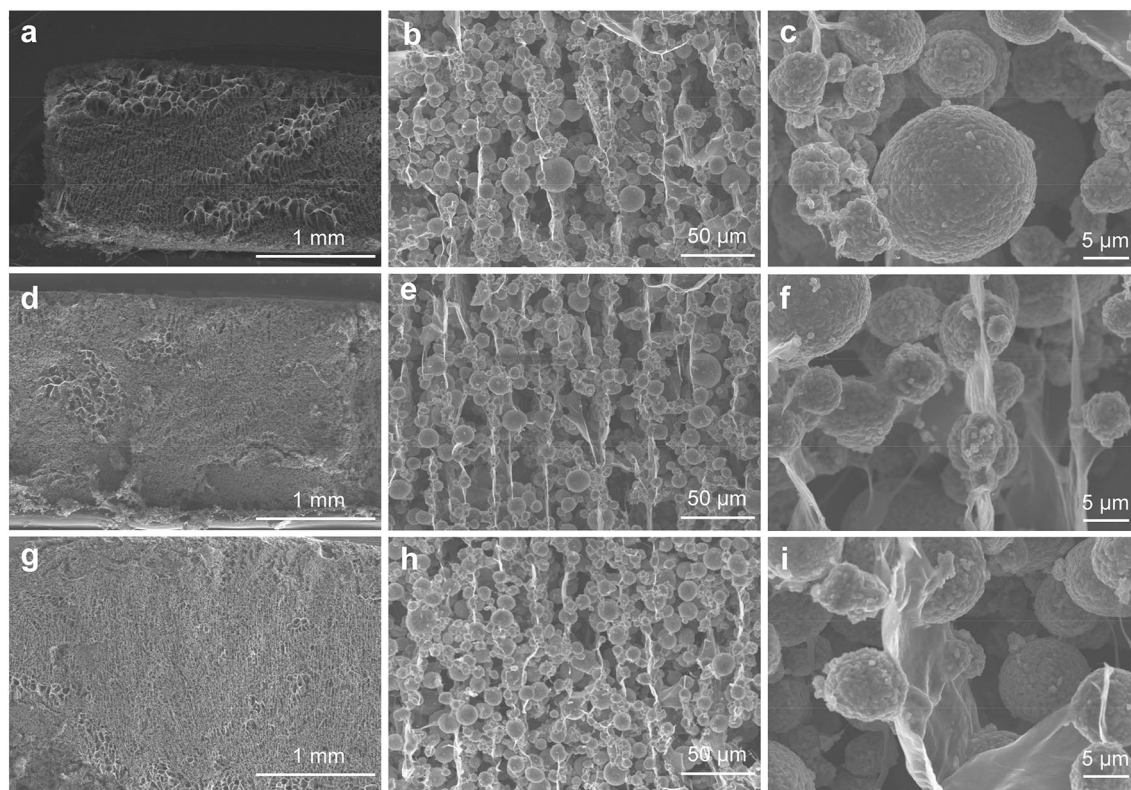
Fig. 2 SEM images of prepared XG-based thickness electrodes with freeze-dried aligned structures (1.25 ml 1 wt% xanthan gum + 2.50 ml 1 wt% guar gum + 3.75 ml 0.4 wt% SWCNT with 5 g NCM811 addition): **a–c** about 1 mm and mass loading of about 100 mg·cm^{-2}; **d–f** about 2 mm and mass loading of about 200 mg·cm^{-2}; **g–i** about 3 mm and mass loading of about 300 mg·cm^{-2}

gum and guar gum contain large amounts of oxygen-containing functional groups and can form a robust biopolymer network which can provide strong mechanical capability to support up to 538 mg·cm^{-2} mass loading of electrode, and further reach an ultra-high areal specific capacity of 93.4 mAh·cm^{-2}.

Further characterizations of the binder and electrode are shown in Fig. 3. Figure 3a shows the dynamic viscosity and shear thinning property of the xanthan gum, guar gum and their mixture. The water-soluble XG mixture displayed an observably higher viscosity than the viscosity measured from single xanthan or guar gum binder, indicating the intermolecular binding effect between xanthan gum and guar gum. The intermolecular synergistic interactions between xanthan gum and guar gum were studied by Fourier transform infrared (FTIR) spectroscopy (Fig. 3b). FTIR spectra of xanthan gum, guar gum and their mixture show a broad absorption band at 3420 cm^{-1}, which can be ascribed to O–H stretching, a peak at 1077 cm^{-1} related to CH$_2$–OH stretching, a peak at 1150 cm^{-1} corresponding to a C–OH stretching mode, an absorption band at 1730 cm^{-1} corresponding to the stretching of the carbonyl (C = O) ester in the acetyl group and an absorption band at 1646 cm^{-1} corresponding to asymmetric C = O stretching in the

carboxylate group [35–37]. Figure 3c, d shows mercury porosimeter for the cumulative pore volume and differential intrusion of the conventional thermal dried electrode and vacuum freeze-dried electrode. By comparing the vacuum-drying against the conventional drying treatments of the thick electrodes with mixed XG gum binder, NCM811 and SWCNT, the total pore volume in the freeze-dried electrode is about 4 times larger than that of conventional drying. Here, the pore diameters are greater in the vacuum freeze-dried electrode (15 μm) than in the conventionally dried electrode (5 μm). This can explain the remaining aligned and open pore structure created by the directional ice templating during the sublimation drying process.

As is shown in Fig. S7, X-ray diffraction (XRD) patterns of the thick electrode can confirm the active materials of NCM particles. As shown in Fig. S3, the thick electrodes (XG binder, NCM and SWCNT) made by conventional thermal drying suffer from rough surface and mechanical integrity, and thus cannot be used for cell fabrication and further test. In this work, NCM811 and Li metal were used as cathode and anode, respectively, to assemble the cell. Figure 4a–c shows the first three cycles of charging and discharging performances of ultra-thick electrodes with mass loading of 101, 245 and 310 mg·cm^{-2}, respectively.
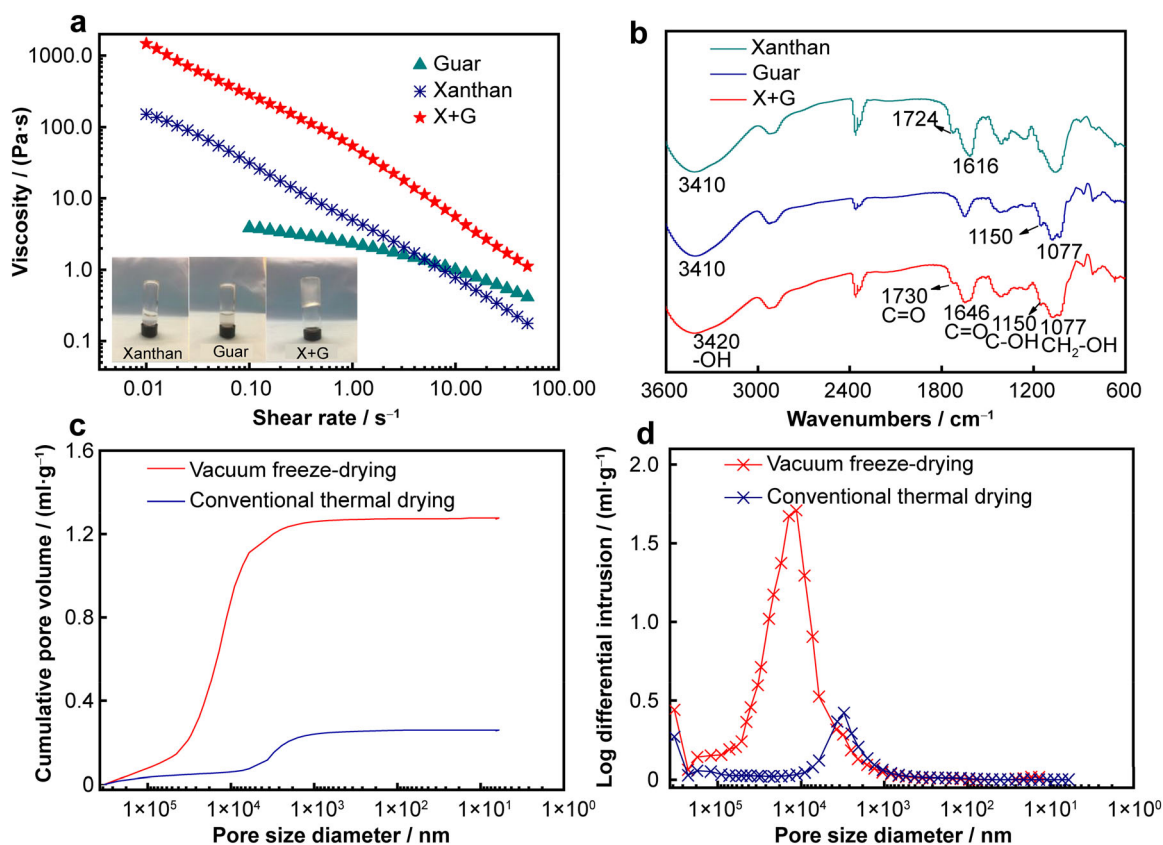
Fig. 3 Properties characterization of binder and thick electrode materials: **a** dynamic viscosity and shear thinning property of xanthan gum, guar gum and XG; **b** FTIR spectra of xanthan gum, guar gum and XG. Mercury porosimeter for **c** cumulative pore volume and **d** differential intrusion of conventionally dried electrode and vacuum freeze-dried electrode

Here, the thick electrode with mass loading of 101 mg·cm^{-2} shows a high discharge capacity of 20.5 mAh·cm^{-2} (203.4 mAh·g^{-1}) and the thick electrode with mass loading of 245 mg·cm^{-2} can achieve a high discharge capacity of 42.6 mAh·cm^{-2} (173.8 mAh·g^{-1}). The areal capacity increases with the increase in the mass loading, the discharge capacity could reach 54.5 mAh·cm^{-2} (176.2 mAh·g^{-1}) when the mass loading goes to 310 mg·cm^{-2}. Their areal capacities are shown in Fig. 4d, and the capacity could maintain 64.4% of its initial capacity after 5 cycles for the thick electrode with mass loading of 310 mg·cm^{-2}. Figures 4f, S8, S9 show the mechanical integrity of the cycled thick electrode, indicating that Li metal anode or electrolyte may be the performance limiting factor of the cell. To further prove this hypothesis, we fabricated the cell with ultra-thick electrode with mass loading of about 538 mg·cm^{-2}. As shown in Fig. 4e, this ultra-thick electrode stopped working after 1 cycle. Later, the performance of the "failed" cathode can be recovered after replacing the cycled Li metal anode with a new Li metal anode and adding some fresh electrolyte. It was worth noting that the cell capacity can almost be fully recovered, and the reused thick electrode could obtain a

capacity of 171.5 mAh·g^{-1}, which nearly approaches its initial capacity (173.7 mAh·g^{-1}). Meanwhile, a thick black film can be observed on the surface of the Li metal anode (Fig. 4e, inset) after taking the old Li metal apart the cell, further revealing that the Li metal pulverization may be a main factor that affects the performance of the cell. The areal capacity and thickness comparison of the NCM thick electrodes with other reported paper are presented in Table S1. It is worth noting that the ultra-thick electrode prepared by our work achieves the highest thickness and area capacity.

In summary, we developed a scalable and sustainable approach to fabricate ultra-thick and ultra-high mass loading electrodes using NCM811, mixed gum binder (xanthan gum and guar gum) and SWCNT via freeze-drying. The electrode manufacturing engineering enables the construction of directional aligned microstructured electrode which can been demonstrated as an efficient approach to accelerate both the electron and ion transport in thick electrodes. The as-prepared ultra-thick electrodes have outstanding advantages of robust mechanical properties and excellent electrochemical kinetics. The robust mechanical properties and aligned structure of the gum
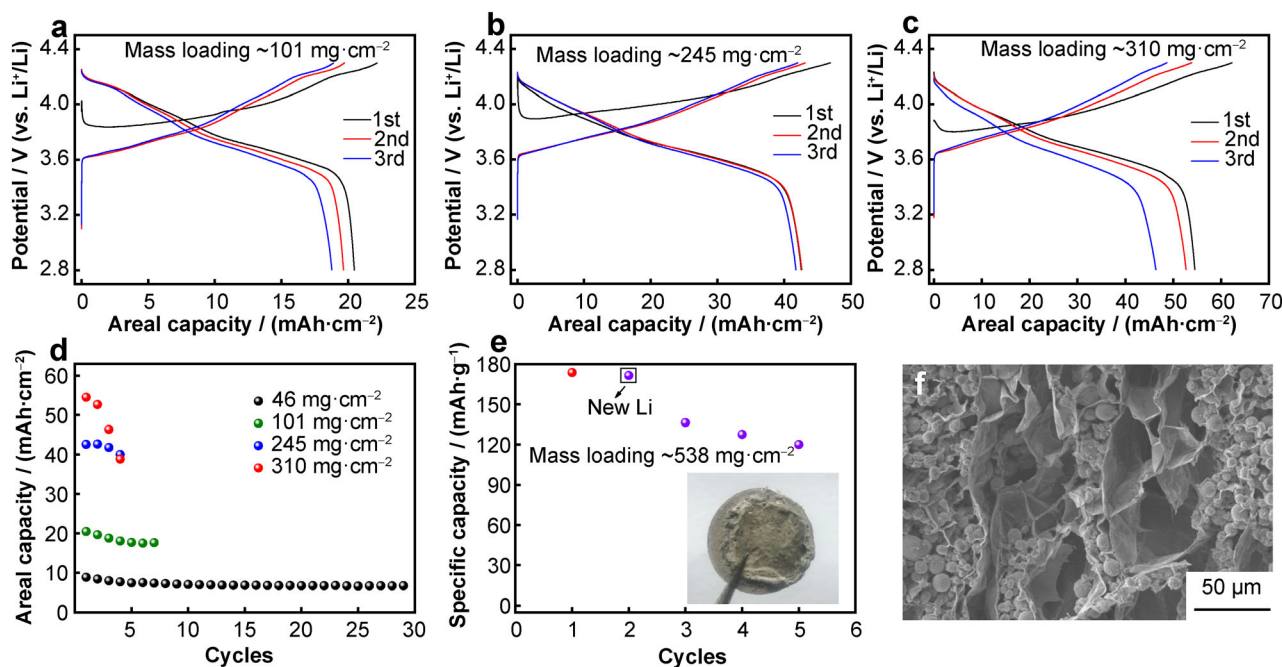
Fig. 4 Electrochemical characterization of ultra-thick electrodes with high mass loading: the first three cycles of charge–discharge curves for thick electrodes at a rate of 0.05C for mass loadings of about **a** 101 mg·cm^{-2}, **b** 245 mg·cm^{-2} and **c** 310 mg·cm^{-2}; **d** cycling performance of ultra-thick electrodes with different mass loadings at a rate of 0.10C (46 mg·cm^{-2}) and 0.05C (101, 245 and 310 mg·cm^{-2}); **e** cycling performance of electrode with mass loading of 538 mg·cm^{-2} and photograph of Li metal counter electrode after cycling (performance can be restored with a new Li metal anode); **f** SEM images of thick electrode after cycling

binder gave rise to a high mass loading electrode of 538 mg·cm^{-2} with an ultra-high areal capacity of 93.4 mAh·cm^{-2}. The way of manufacturing processes to fabricate ultra-thick electrodes using gum binder and freeze-drying that can retain 99.5% of the active material, and provide an effective way to increase areal capacity. The discharge areal capacity could reach 93.4 mAh·cm^{-2} when the mass loading goes up to 538 mg·cm^{-2}, improved by 30 times compared to that of the commercial electrode. This work sheds lights on the electrode manufacturing to improve the battery energy density, yet opening a new avenue to construct high-performance battery and other energy storage devices.

References

[1] Liu Y, Zhu Y, Cui Y. Challenges and opportunities towards fast-charging battery materials. Nat Energy. 2019;4(7):540.

[2] Billaud J, Bouville F, Magrini T, Villevieille C, Studart AR. Magnetically aligned graphite electrodes for high-rate performance Li-ion batteries. Nat Energy. 2016;1(8):1.

[3] Yang S, He R, Zhang Z, Cao Y, Gao X, Liu X. Chain: cyber hierarchy and interactional network enabling digital solution for battery full-lifespan management. Matter. 2020;3(1):27.

[4] Yang R, Zhang XJ, Fan TF, Jiang DP, Wang Q. Improved electrochemical performance of ternary Sn–Sb–Cu nanospheres as anode materials for lithium-ion batteries. Rare Met. 2020; 39(10):1159.

[5] Jaiser S, Müller M, Baunach M, Bauer W, Scharfer P, Schabel W. Investigation of film solidification and binder migration during drying of Li-ion battery anodes. J Power Sources. 2016; 318(30):210.

[6] Baunach M, Jaiser S, Schmelzle S, Nirschl H, Scharfer P, Schabel W. Delamination behavior of lithium-ion battery anodes: influence of drying temperature during electrode processing. Dry Technol. 2016;34(4):462.

[7] Liu J, Galpaya DGD, Yan L, Sun M, Lin Z, Yan C, Liang C, Zhang S. Exploiting a robust biopolymer network binder for an ultrahigh-areal-capacity Li-S battery. Energy Environ Sci. 2017; 10(3):750.

[8] Wang H, Zheng P, Yi H, Wang Y, Yang Z, Lei Z, Chen Y, Deng Y, Wang C, Yang Y. Low-cost and environmentally friendly biopolymer binders for Li-S batteries. Macromolecules. 2020; 53(19):8539.

[9] Kuang Y, Chen C, Kirsch D, Hu L. Thick electrode batteries: principles, opportunities, and challenges. Adv Energy Mater. 2019;9(33):1901457.

[10] Shi B, Shang Y, Pei Y, Pei S, Wang L, Heider D, Zhao YY, Zheng C, Yang B, Yarlagadda S, Chou TW, Fu KK. Low Tortuous, highly conductive, and high-areal-capacity battery electrodes enabled by through-thickness aligned carbon fiber framework. Nano Lett. 2020;20(7):5504.

[11] Kim JM, Park CH, Wu Q, Lee SY. 1D building blocks-intermingled heteronanomats as a platform architecture for

high-performance ultrahigh-capacity lithium-ion battery cathodes. Adv Energy Mater. 2016;6(2):1501594.

[12] Chen Y, Wang Y, Wang Z, Zou M, Zhang H, Zhao W, Yousaf M, Yang L, Cao A, Han PRS. Densification by compaction as an effective low-cost method to attain a high areal lithium storage capacity in a CNT@Co_3O_4 sponge. Adv Energy Mater. 2018; 8(19):1702981.

[13] Pang GY, Zhuang WD, Bai XT, Ban LQ, Zhao CR, Sun XY. Research advances of co-free and Ni-rich $LiNi_xMn_{1-x}O_2$ ($0.5{<}x{<}1$) cathode materials. Chin J Rare Met. 2020;44(9):996.

[14] Braun PV, Cho J, Pikul JH, King WP, Zhang H. High power rechargeable batteries. Curr Opin Solid State Mater Sci. 2012; 16(4):186.

[15] Shen F, Luo W, Dai J, Yao Y, Zhu M, Hitz E, Tang Y, Chen Y, Sprenkle VL, Li X, Hu L. Ultra-thick, low-tortuosity, and mesoporous wood carbon anode for high-performance sodium-ion batteries. Adv Energy Mater. 2016;6(14):1600377.

[16] Huang SF, Lv Y, Tie D, Yu Y, Zhao YF. Realizing simultaneously enhanced energy and power density full-cell construction using mixed hard carbon/$Li_4Ti_5O_{12}$ electrode. Rare Met. 2021;40(1):65.

[17] Cheng HM, Li F. Charge delivery goes the distance. Science. 2017;356(6338):582.

[18] Sun H, Zhu J, Baumann D, Peng L, Xu Y, Shakir I, Huang Y, Duan X. Hierarchical 3D electrodes for electrochemical energy storage. Nat Rev Mater. 2019;4(1):45.

[19] Ji H, Zhang L, Pettes MT, Li H, Chen S, Shi L, Piner R, Ruoff RS. Ultrathin graphite foam: a three-dimensional conductive network for battery electrodes. Nano Lett. 2012;12(5):2446.

[20] Xu J, Tan Z, Zeng W, Chen G, Wu S, Zhao Y, Ni K, Tao Z, Ikram M, Ji H, Zhu Y. A hierarchical carbon derived from sponge-templated activation of graphene oxide for high-performance supercapacitor electrodes. Adv Mater. 2016;28(26):5222.

[21] Zhou L, Ning W, Wu C, Zhang D, Wei W, Ma J, Li C, Chen L. 3D-printed microelectrodes with a developed conductive network and hierarchical pores toward high areal capacity for microbatteries. Adv Mater Technol. 2019;4(2):1800402.

[22] Sun C, Liu S, Shi X, Lai C, Liang J, Chen Y. 3D printing nanocomposite gel-based thick electrode enabling both high areal capacity and rate performance for lithium-ion battery. Chem Eng J. 2020;381:122641.

[23] Zhang ZJ, Zhao J, Qiao ZJ, Wang JM, Sun SH, Fu WX, Zhang XY, Yu ZY, Dou YH, Kang JL, Yuan D, Feng YZ, Ma JM. Nonsolvent-induced phase separation-derived TiO_2 nanotube arrays/porous Ti electrode as high-energy-density anode for lithium-ion batteries. Rare Met. 2020;40(2):393.

[24] Long JW, Dunn B, Rolison DR, White HS. Three-dimensional battery architectures. Chem Rev. 2004;104(10):4463.

[25] Zhang H, Yu X, Braun PV. Three-dimensional bicontinuous ultrafast-charge and-discharge bulk battery electrodes. Nat Nanotechnol. 2011;6(5):277.

[26] Chen C, Zhang Y, Li Y, Dai J, Song J, Yao Y, Gong Y, Kierzewski I, Xie J, Hu L. All-wood, low tortuosity, aqueous, biodegradable supercapacitors with ultra-high capacitance. Energy Environ Sci. 2017;10(2):538.

[27] Lee SY, Cho SJ, Choi KH, Yoo JT, Kim JH, Lee YH, Chun SJ, Park SB, Choi DH, Wu Q, Lee SY. Hetero-nanonet rechargeable paper batteries: toward ultrahigh energy density and origami foldability. Adv Funct Mater. 2015;25(38):6029.

[28] Li H, Tao Y, Zheng X, Luo J, Kang F, Cheng HM, Yang QH. Ultra-thick graphene bulk supercapacitor electrodes for compact energy storage. Energy Environ Sci. 2016;9(10):3135.

[29] Wang B, Ryu J, Choi S, Song G, Hong D, Hwang C, Chen X, Wang B, Li W, Song HK, Park S, Ruoff RS. Folding graphene film yields high areal energy storage in lithium-ion batteries. ACS Nano. 2018;12(2):1739.

[30] Behr S, Amin R, Chiang YM, Tomsia AP. Highly-structured, additive-free lithium-ion cathodes by freeze-casting technology. CFI Ceram Forum. 2015;92(4):39.

[31] Sander JS, Erb RM, Li L, Gurijala A, Chiang YM. High-performance battery electrodes via magnetic templating. Nat Energy. 2016;1(8):1.

[32] Shi Y, Zhou X, Zhang J, Bruck AM, Bond AC, Marschilok AC, Takeuchi KJ, Takeuchi ES, Yu G. Nanostructured conductive polymer gels as a general framework material to improve electrochemical performance of cathode materials in li-ion batteries. Nano Lett. 2017;17(3):1906.

[33] Sereno NM, Hill SE, Mitchell JR. Impact of the extrusion process on xanthan gum behaviour. Carbohydr Res. 2007;342(10): 1333.

[34] Morris ER, Nishinari K, Rinaudo, M. Gelation of gellan-a review. Food Hydrocoll. 2012; 28(2):373.

[35] Mudgil D, Barak S, Khatkar BS. X-ray diffraction, IR spectroscopy and thermal characterization of partially hydrolyzed guar gum. Int J Biol Macromol. 2012;50(4):1035.

[36] Velimirovic M, Chen H, Simons Q, Bastiaens L. Reactivity recovery of guar gum coupled mZVI by means of enzymatic breakdown and rinsing. J Contam Hydrol. 2012;142–143:1.

[37] Maia AMS, Silva HVM, Curti PS, Balaban RC. Study of the reaction of grafting acrylamide onto xanthan gum. Carbohydr Polym. 2012;90(2):778.